Intersubband pairing induced Fulde-Ferrell phase in metallic nanofilms

P. Wójcik,[1,*] M. P. Nowak,[2] and M. Zegrodnik[2]

[1]*AGH University of Science and Technology, Faculty of Physics and Applied Computer Science, al. A. Mickiewicza 30, 30-059 Krakow, Poland*

[2]*AGH University of Science and Technology, Academic Centre for Materials and Nanotechnology, al. A. Mickiewicza 30, 30-059 Krakow, Poland*

(Received 12 April 2019; revised manuscript received 6 June 2019; published 15 July 2019)

We consider a freestanding metallic nanofilm with a predominant intersubband pairing which emerges as a result of the confinement in the growth direction. We show that the Fermi wave vector mismatch between the subbands, detrimental to the intersubband pairing, can be compensated by the nonzero center-of-mass momentum of the Cooper pairs. This leads to the spontaneous appearance of the intersubband Fulde-Ferrell (IFF) state, even in the absence of an external magnetic field. Our study of the intrasubband pairing channel on the stability of the IFF phase shows that the former strongly competes with the intersubband pairing, which prohibits the coexistence of the two superconducting phases. Interestingly, upon application of the magnetic field we find a transition to an exotic mixed spin-singlet subband-triplet and spin-triplet subband-singlet paired state. Finally, we discuss the possibility of existence of the IFF pairing in novel superconducting materials.

DOI: 10.1103/PhysRevB.100.045409

I. INTRODUCTION

In the past decade, the study of superconductors in the nanoscale regime has evolved into one of the most active research directions in the solid-state physics. This was mostly driven by the rapid progress in growth and characterization techniques which allow metallic films and other types of superconducting materials to be fabricated with atomic precision [1–3]. In metallic nanofilms, due to the strong confinement of electrons in the growth direction, the Fermi surface splits into series of subbands that result in multiband superconductivity similar to that observed in superconductors such as MgB_2 [4–7] and iron pnictides [8–11]. The multiband character of superconductivity in metallic nanofilms was confirmed by measurements of the critical temperature [12–14] and magnetic field [15,16] oscillations as a function of the nanofilm thickness. This behavior was explained as resulting from the Van Hove singularities occurring each time when the bottom of the subband passes through the Fermi level (Lifshitz transition) [17–19].

When the material becomes thin enough, the confinement affects not only the electronic spectrum but also the phononic degrees of freedom. The phonon dispersion in thin films strongly deviates from that observed in the bulk [20], which changes the electron-phonon coupling. Determination of the electron-phonon coupling in individual subbands and between them in metallic nanofilms is still an open issue from both theoretical and experimental points of view. In particular, when the energy between electronic states (subbands) becomes smaller than the Debye window [21], the unconventional intersubband pairing can appear. In this paper, we show that in metallic nanofilms, the existence of such an exotic intersubband pairing can spontaneously induce a superconducting phase with a finite center-of-mass momentum of the Cooper pairs.

The finite-momentum pairing was originally introduced in the 1960s by Fulde and Ferrell [22] as well as Larkin and Ovchinnikov [23] as resulting from the paramagnetic effect. In the external magnetic field the Zeeman splitting of the Fermi surface generates the Fermi wave vector mismatch between spin-up and spin-down electrons, which is detrimental for the pairing of electrons in the spin-singlet state. The Fermi wave vector mismatch can be compensated by the nonzero center-of-mass momentum of the Copper pairs leading to the Fulde-Ferrell (FF) phase [24–27]. Although the physics standing behind the finite-momentum Cooper pairing is relatively transparent, its experimental observation turned out to be extremely challenging. This is mainly due to the dominant role of the orbital effects which suppress the critical field well below the range of the FF phase stability [28]. For this reason, the existence of this unconventional paired state has been proposed to appear in two-dimensional (2D) organic superconductors [29–32] and ultrathin films [33–35] subject to an in-plane magnetic field, where the orbital effects are strongly suppressed by the confinement in the growth direction. Alternatively, the FF phase is believed to appear in heavy-fermion systems [36–39] where the orbital effects are suppressed by the high effective mass or superconducting nanowires [40,41]. So far, in the ongoing debate on the stability of the FF phase [42], strong experimental evidence of the finite-momentum pairing has been provided only in 2D organic superconductors [31, 43–45] and superconductor/ferromagnet [46] (topological insulator [47,48]) junctions for which the FF phase is formed in the proximitized part of the junction.

In this paper, we show that the FF phase can appear spontaneously (without the magnetic field) in superconducting metallic nanofilms as a result of the quantization of the electronic bands in the growth direction. When the

*pawel.wojcik@fis.agh.edu.pl

energy between quantized electronic states is smaller than the phonon bandwidth, for sufficiently large electron-phonon interaction [49] the electrons from different bands can create Cooper pairs. Then, the Fermi wave vector mismatch between the subbands is compensated by the nonzero center-of-mass momentum of the Cooper pairs, leading to the spontaneous FF phase formation induced by the intersubband pairing.

The structure of the paper is as follows. In Sec. II we introduce the theoretical model of the nonzero momentum pairing in metallic nanofilms. In Sec. III we present our results both in the absence and in the presence of the magnetic field. Conclusions and outlook are provided in Sec. V.

II. THEORETICAL MODEL

A. FF phase in a metallic nanofilm

We consider Pb(111) freestanding nanofilms with predominant intersubband electron-phonon coupling. The first-principles calculations [50] of the quantized band structure for Pb nanofilms showed that the quantum size effect in the (111) direction can be well described only by the quantum well states centered at the L point of the Brillouin zone, where the energy dispersion is nearly parabolic. Based on those results, here we use the parabolic band approximation. For simplicity, we consider the two lowest subbands, assuming that they are separated by the energy ΔE. The two-band model allows us to underline the sole role of the intersubband pairing without any disturbances resulting from Cooper pairs tunneling to other subbands. A schematic illustration of pairing in the considered model is presented in Fig. 1.

For $\mathbf{H} = 0$ and small intersubband coupling strength, the superconducting state is created as a result of pairing between electrons with opposite spins and momenta within the subbands, $(1, \mathbf{k}, \uparrow) \Leftrightarrow (1, -\mathbf{k}, \downarrow)$ and $(2, \mathbf{k}, \uparrow) \Leftrightarrow (2, -\mathbf{k}, \downarrow)$. If we increase the intersubband coupling, a new pairing channel opens, where electrons from different subbands form the Cooper pairs $(1, \mathbf{k}, \uparrow) \Leftrightarrow (2, -\mathbf{k} + \mathbf{Q}, \downarrow)$. In such a case, the wave vector mismatch between electrons with opposite spins is compensated by the nonzero momentum of the pairs $\mathbf{Q}$, leading to the spontaneous (without the magnetic field) FF phase [Fig. 1(a)], in which not all of the particles at the Fermi surface are paired. The further increase of the intersubband coupling above a critical value leads to a situation in which the pairing region in reciprocal space is relatively large, meaning that the Fermi wave vector mismatch cannot prevent the electrons from pairing. In such a scenario, the electrons from the more populated subband are moved to the less populated one, and the intersubband pairing with zero momentum $\mathbf{Q} = 0$ is preferable.

If we apply the magnetic field $\mathbf{H} \neq 0$ [Fig. 1(b)], both the subbands split as a result of the Zeeman effect. The wave vector mismatch between electrons with opposite spins appears separately in each subband, which may result in the finite-momentum pairing in each of them. In general, the Cooper pair momenta $\mathbf{Q}$ for both the subbands and between them can be different, leading to the FF phase which is a superposition of phases with three different $\mathbf{Q}$ vectors (periods of the energy gap oscillations in real space). In this case, the appearance of the intra- and intersubband FF phases as well as their coexistence is determined by the spin-splitting energy and the energy separation ΔE. In particular, the Zeeman splitting can compensate the energy ΔE between states $(1, \uparrow)$ and $(2, \downarrow)$, making the pairing between them preferable, while the pairing between the spin-reversed states $(1, \downarrow)$ and $(2, \uparrow)$ is destroyed by the large vector mismatch between the states at the Fermi level, which increases with the increasing magnetic field.

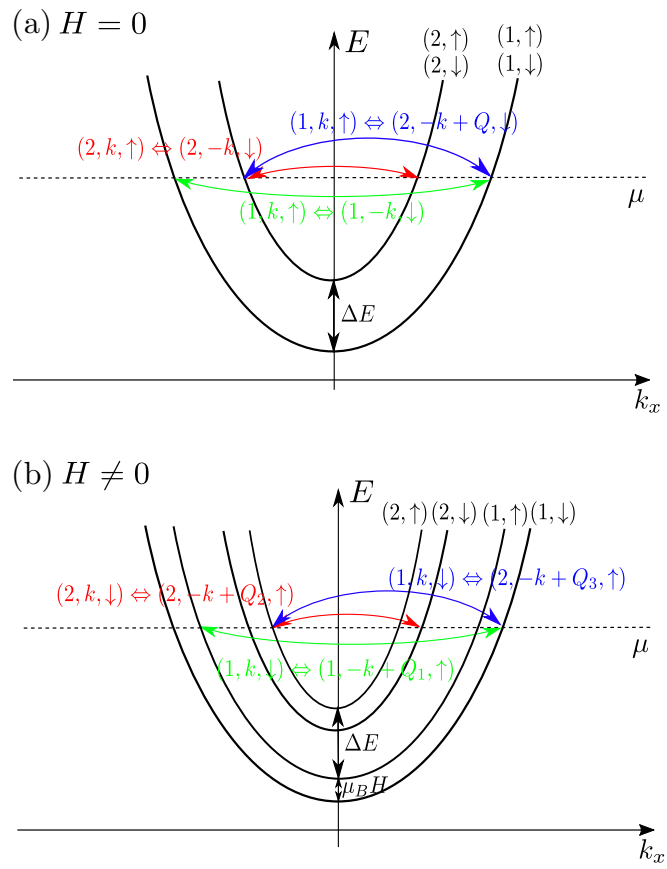

FIG. 1. Schematic illustration of pairing in the two-band model (cross section along $k_y = 0$) for magnetic field (a) $H = 0$ and (b) $H \neq 0$. Electronic states from opposite sides of the Fermi surface, forming Cooper pairs, are connected by arrows. The intersubband finite-momentum pairing is marked by the blue arrows. The horizontal dashed line denotes the Fermi level μ.

B. Two-band model with intersubband pairing

We start from the general form of the mean-field BCS Hamiltonian in the presence of external in-plane magnetic field $\mathbf{H} = (H, 0, 0)$,

$$\hat{\mathcal{H}} = \sum_{\sigma} \int d^3r \hat{\Psi}^{\dagger}(\mathbf{r}, \sigma) \hat{H}_e^{\sigma} \hat{\Psi}(\mathbf{r}, \sigma) + \int d^3r [\Delta(\mathbf{r}) \hat{\Psi}^{\dagger}(\mathbf{r}, \uparrow) \hat{\Psi}^{\dagger}(\mathbf{r}, \downarrow) + \text{H.c.}] + \int d^3r \frac{|\Delta(\mathbf{r})|^2}{g}, \quad (1)$$

where σ corresponds to the spin state $(\uparrow, \downarrow)$, g is the phonon-mediated electron-electron coupling constant, $\hat{H}_e^{\sigma}$ is

the single-electron Hamiltonian, and $\Delta(\mathbf{r})$ is the superconducting gap parameter in real space defined as

$$\Delta(\mathbf{r}) = -g\langle\hat{\Psi}(\mathbf{r},\downarrow)\hat{\Psi}(\mathbf{r},\uparrow)\rangle. \tag{2}$$

In the two-band model the field operators have the form

$$\hat{\Psi}(\mathbf{r},\sigma) = \sum_{\mathbf{k}}[\phi_{1\mathbf{k}}(\mathbf{r})\,\hat{c}_{1\mathbf{k}\sigma} + \phi_{2\mathbf{k}}(\mathbf{r})\,\hat{c}_{2\mathbf{k}\sigma}], \tag{3}$$

$$\hat{\Psi}^{\dagger}(\mathbf{r},\sigma) = \sum_{\mathbf{k}}[\phi^{*}_{1\mathbf{k}}(\mathbf{r})\,\hat{c}^{\dagger}_{1\mathbf{k}\sigma} + \phi^{*}_{2\mathbf{k}}(\mathbf{r})\,\hat{c}^{\dagger}_{2\mathbf{k}\sigma}], \tag{4}$$

where $\hat{c}_{n\mathbf{k}\sigma}(\hat{c}^{\dagger}_{n\mathbf{k}\sigma})$, with $n = (1, 2)$, is the annihilation (creation) operator for an electron with spin σ in the subband n characterized by the wave vector $\mathbf{k}$ and $\phi_{n\mathbf{k}}(\mathbf{r})$ are the single-electron eigenfunctions of the Hamiltonian $\hat{H}^{\sigma}_{e}$.

The FF phase, induced either by the intersubband coupling or by the Zeeman splitting, is characterized by the pairing with the nonzero momentum $(\mathbf{k},\uparrow) \Leftrightarrow (-\mathbf{k}+\mathbf{Q},\downarrow)$. The two-band Hamiltonian with the finite-momentum pairing takes the form

$$\hat{\mathcal{H}}^{\mathbf{Q}} = \sum_{\mathbf{k}}\hat{\mathbf{f}}^{\dagger}_{\mathbf{k},\mathbf{Q}}H^{\mathbf{Q}}_{\mathbf{k}}\hat{\mathbf{f}}_{\mathbf{k},\mathbf{Q}} + \sum_{\mathbf{k}}(\xi_{1,-\mathbf{k}+\mathbf{Q},\downarrow} + \xi_{2,-\mathbf{k}+\mathbf{Q},\downarrow}) + \sum_{n,m=1,2}\frac{|\Delta^{\mathbf{Q}}_{n,m}|^2}{g}, \tag{5}$$

where $\hat{\mathbf{f}}^{\dagger}_{\mathbf{k},\mathbf{Q}} = (\hat{c}^{\dagger}_{1,\mathbf{k},\uparrow}, \hat{c}_{1,-\mathbf{k}+\mathbf{Q},\downarrow}, \hat{c}^{\dagger}_{2,\mathbf{k},\uparrow}, \hat{c}_{2,-\mathbf{k}+\mathbf{Q},\downarrow})$ is the composite vector operator and

$$H^{\mathbf{Q}}_{\mathbf{k}} = \begin{pmatrix} \xi_{1,\mathbf{k},\uparrow} & \Gamma^{\mathbf{Q}}_{1,1} & 0 & \Gamma^{\mathbf{Q}}_{1,2} \\ \Gamma^{\mathbf{Q}}_{1,1} & -\xi_{1,-\mathbf{k}+\mathbf{Q},\downarrow} & \Gamma^{\mathbf{Q}}_{2,1} & 0 \\ 0 & \Gamma^{\mathbf{Q}}_{2,1} & \xi_{2,\mathbf{k},\uparrow} & \Gamma^{\mathbf{Q}}_{2,2} \\ \Gamma^{\mathbf{Q}}_{1,2} & 0 & \Gamma^{\mathbf{Q}}_{2,2} & -\xi_{2,-\mathbf{k}+\mathbf{Q},\downarrow} \end{pmatrix}. \tag{6}$$

In the above Hamiltonian, $\xi_{n,\mathbf{k}}$ are the single-particle energies, which, in parabolic band approximation, are given by

$$\begin{aligned} \xi_{1,\mathbf{k},\sigma} &= E_0 + \frac{\hbar^2(k_x^2+k_y^2)}{2m} + s\mu_B H - \mu, \\ \xi_{2,\mathbf{k},\sigma} &= E_0 + \frac{\hbar^2(k_x^2+k_y^2)}{2m} + s\mu_B H + \Delta E - \mu, \end{aligned} \tag{7}$$

where m is the electron mass, μ is the Fermi energy, $s = \pm 1$ for the spin index $\sigma = (\uparrow,\downarrow)$, μ_B is the Bohr magneton, $\mathbf{k} = (k_x, k_y)$, and E_0 is the bottom of the lower subband, assumed to be the reference energy ($E_0 = 0$). Due to the strong confinement in the growth direction, the orbital effects from the in-plane magnetic field can be neglected.

The intra- and intersubband superconducting gap parameters $\Gamma^{\mathbf{Q}}_{n,m}$ are expressed by

$$\Gamma^{\mathbf{Q}}_{n,m} = -g\sum_{n',m'=1,2}V^{n',m'}_{n,m}\Delta^{\mathbf{Q}}_{n',m'}, \tag{8}$$

where the interaction matrix elements

$$V^{n',m'}_{n,m} = \int d^3r\phi^{*}_{n\mathbf{k}}(\mathbf{r})\phi^{*}_{m\mathbf{k}}(\mathbf{r})\phi_{n'\mathbf{k}}(\mathbf{r})\phi_{m'\mathbf{k}}(\mathbf{r}) \tag{9}$$

and

$$\Delta^{\mathbf{Q}}_{n,m} = {\sum_{k}}'\langle\hat{c}_{n,-\mathbf{k}+\mathbf{Q},\downarrow}\hat{c}_{m,\mathbf{k},\uparrow}\rangle. \tag{10}$$

The primed sum in (10) means that the summation is carried out only if both the single-electron states $\xi_{n,\mathbf{k}}$ and $\xi_{m,\mathbf{k}}$ are located inside the Debye window $[\mu - \hbar\omega_D, \mu + \hbar\omega_D]$, where ω_D is the Debye frequency.

Note that in the parabolic band approximation $V^{n',m'}_{n,m}$ does not depend on the $\mathbf{k}$ vector. Moreover, due to the symmetry of the single-electron eigenfunctions (we assume the hard-wall potential) $V^{n,m}_{n,n} = V^{m,n}_{n,m} = V^{m,m}_{n,m} = V^{n,n}_{n,m} = 0$, and $V^{m,m}_{n,n} = V^{n,n}_{m,m} = V^{n,m}_{n,m} = V^{m,n}_{n,m}$. This, in turn, reduces the interaction matrix to three nonzero elements: two intrasubband coupling constants, which we assumed to be equal $V = V^{11}_{11} = V^{22}_{22}$, and the intersubband coupling constant, $V_{12} = V^{22}_{11}$. The interaction matrix elements V and V_{12} determine the effective electron-electron interaction by changing the g parameter for the intra- and intersubband pairing. In the following part of the paper we treat V and V_{12} as dimensionless parameters which control the pairing by rescaling g (expressed in eV).

The numerical diagonalization of (6) leads to the quasiparticle energies $\lambda_{i,\mathbf{k},\mathbf{Q}}$ $(i = 1,\ldots,4)$ which are then used to derive the free-energy functional in a standard statistical-mechanical manner,

$$F(\mathbf{Q}) = -k_BT\sum_{\mathbf{k},i=1\ldots4}\ln\left[1+\exp\left(\frac{\lambda_{i,\mathbf{k},\mathbf{Q}}}{k_BT}\right)\right] + \sum_{\mathbf{k}}(\xi_{1,-\mathbf{k}+\mathbf{Q},\downarrow} + \xi_{2,-\mathbf{k}+\mathbf{Q},\downarrow} + \lambda_{2,\mathbf{k},\mathbf{Q}} + \lambda_{4,\mathbf{k},\mathbf{Q}}) + \sum_{i,j=1,2}\frac{|\Delta^{\mathbf{Q}}_{ij}|^2}{g} + \mu N, \tag{11}$$

where N is the number of electrons. The pairing energies $\Gamma^{\mathbf{Q}}_{n,m}$ are obtained by solving the set of self-consistent equations, while the $\mathbf{Q}$ vector is determined by minimizing the free energy of the system, Eq. (11).

The calculations were carried out for material parameters corresponding to Pb: $m = 1$, $gN_{\text{bulk}} = 0.18$, where $N_{\text{bulk}} = mk_F/(2\pi^2\hbar^2)$ is the bulk density of the single-electron states at the Fermi level, $\hbar\omega_D = 32.31$ meV and $\mu \gg \Delta E, E_0$.

III. RESULTS

In the first part of our analysis, we focus on the intersubband pairing and the formation of spontaneous FF phase. For the sake of simplicity, we initially consider a situation with $V = 0$ (no intrasubband pairing). The influence of the latter and the case of nonzero external magnetic field are analyzed in the following part of the paper.

In Fig. 2(a) we show the phase diagram in the $(V_{12}, \Delta E)$ plane, with the SC gap marked by the colors. As one can see, significant stability regions of the normal state (NS) and intersubband superconducting phase (ISP) appear in the diagram. The energy separation between the bands has a detrimental influence on the intersubband pairing as it introduces the Fermi wave vector mismatch between the paired electrons. Different energies of the band bottom with respect to the Fermi energy results in disproportion between the number of particles in each of them. In such a case the pairing becomes energetically unfavorable since not all particles can be paired. Nevertheless,

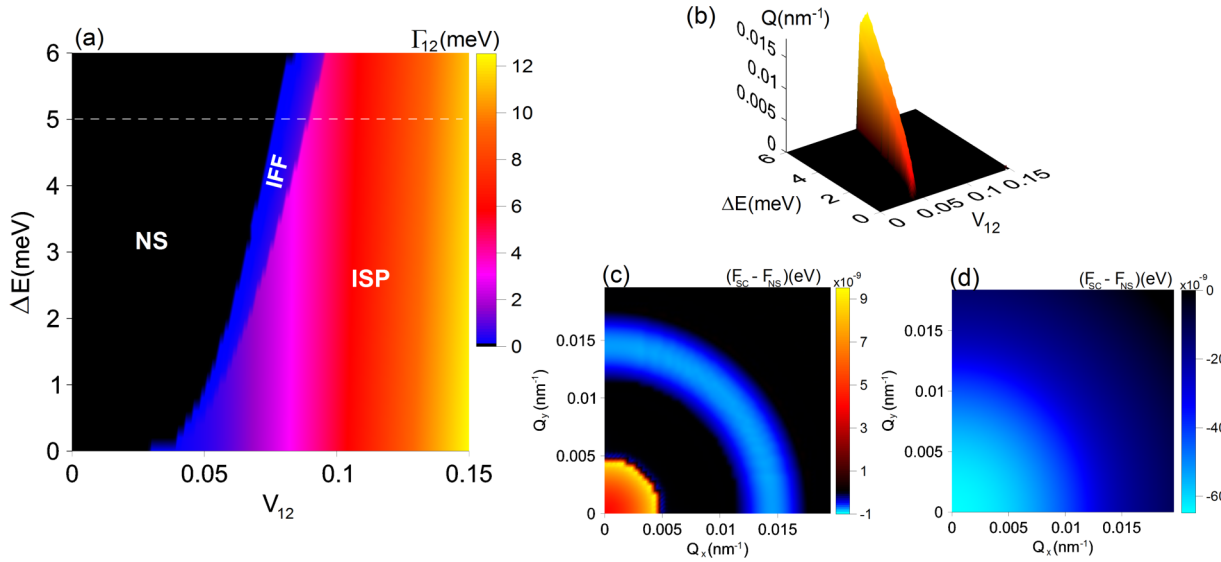

FIG. 2. (a) The phase diagram in the $(V_{12}, \Delta E)$ plane, where one can distinguish the regions of NS (normal state), IFF (intersubband Fulde-Ferrell phase), and ISP (intersubband paired phase). The dashed horizontal line denotes $\Delta E = 5$ meV, chosen for further analysis. (b) The Cooper pair momentum, which minimizes the energy of the system, as a function of both ΔE and V_{12}. (c) and (d) The free energy of the system as a function of the Cooper pair momentum $\mathbf{Q} = (Q_x, Q_y)$ for two selected values of the interband pairing strength V_{12}, for which the IFF and ISP phases are stable, respectively.

for nonzero ΔE and high enough values of V_{12} the width of the pairing region around the Fermi surfaces is relatively large, meaning that the Fermi wave vector mismatch no longer prevents the particles from forming the Cooper pairs. In such a situation, the particles from the more populated subband are transferred to the less populated one, and no unpaired particles are left [49]. Those two effects lead to opening of the gap across the full Fermi surface. The resulting ISP phase resembles a BCS superconductor, except here the Cooper pairs are formed by particles from two different subbands.

An interesting region lies in between NS and ISP, for which the intersubband pairing is already too small to induce a fully gapped paired state; however, superconductivity can still appear in the form of the intersubband Fulde-Ferrell phase (IFF). In the latter, the Fermi wave vector mismatch between the two subbands is compensated by the nonzero center-of-mass momentum of the Cooper pairs, which leads to a nonhomogeneous SC gap with a small depairing region in the Brillouin zone, occupied by the unpaired electrons. In Fig. 2(b) we show the values of the Cooper pair momenta which correspond to the minimum of the free energy. Since we are working in the parabolic band approximation, the direction of the $\mathbf{Q}$ vector can be chosen arbitrarily. This is clearly seen in Figs. 2(c) and 2(d), where the free energy of the system is plotted as a function of both Q_x and Q_y for two selected values of V_{12}. One should note that the obtained rotational symmetry is also a result of the chosen pairing symmetry, which is assumed to be s wave in our case. In general, for other pairing symmetries such as d-wave the rotational symmetry in the (Q_x, Q_y) space can be broken [51,52]. As can be seen, for the situation shown in Fig. 2(d) the nonzero Cooper pairing is not energetically favorable since the energy of the system increases with increasing $\mathbf{Q}$. On the other hand, the energy minimum for nonzero $\mathbf{Q}$ shown in Fig. 2(c) signals the possibility of nonzero momentum pairing. In such situations the SC gap parameter changes its phase in real space as one moves along the direction determined by the modulation vector. The discontinuity in Γ_{12} at the border between ISP and IFF indicates a first order phase transition between the two. Such behavior is also reported for the case of the conventional Fulde-Ferrell phase induced by the presence of an external magnetic field [24]. However, here the nonzero momentum pairing appears spontaneously between two subbands without the application of an external magnetic field.

Our simulations for nonzero temperatures (not shown) demonstrate that the stability region of the IFF phase gradually decreases with increasing temperature, whereas the phase transition between the IFF phase and the ISP phase is noncontinuous, which is indicated by a sudden drop in the gap parameter Γ_{12}.

Next, we consider the influence of the intrasubband pairing on the phase diagram analyzed so far. The situation corresponding to both $V_{12} \neq 0$ and $V \neq 0$ is shown in Fig. 3 for $\Delta E = 5$ meV [marked by the horizontal line in Fig. 2(a)]. Since the calculations including the nonzero momentum pairing are highly time-consuming, we start from the simplified phase diagram with $\mathbf{Q} = 0$. Figure 3(a) presents relatively large regions of stability of the intersubband superconducting state (ISP) as well as the intrasubband paired phase. In the latter we report almost equal superconducting gaps in the two subbands [equal subband pairing (ESP)], $\Delta_{11} \approx \Delta_{22}$, in spite of the nonzero value of the ΔE parameter. The equality of energy gaps is due to relatively high value of the chemical potential with respect to ΔE taken in the calculations. At the transition between intrasubband and intersubband paired phases the superconducting gap is enhanced. It should be noted that for the considered system there is a strong detrimental influence of the intrasubband pairing on the intersubband pair formation. That is why there is no region where the two phases coexist in the diagram. This fact can be understood

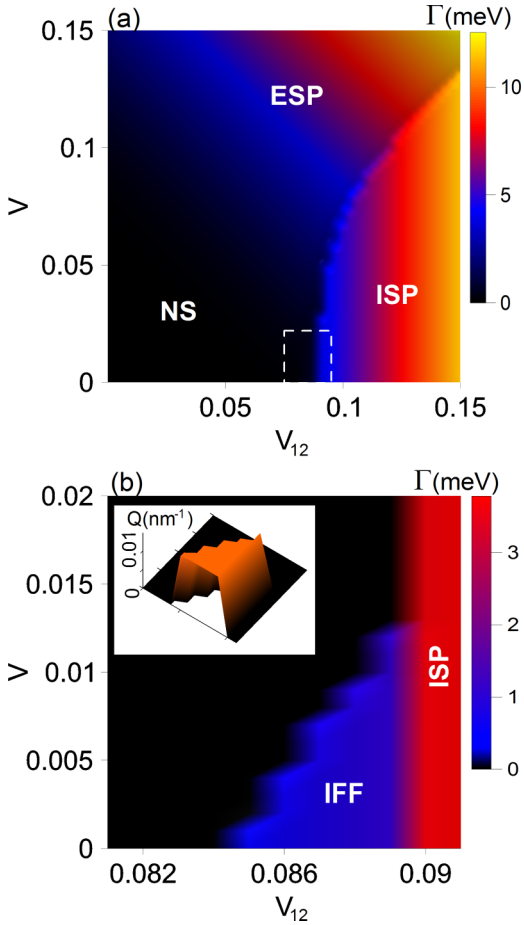

FIG. 3. (a) The superconducting gap parameter as a function of both inter- and intrasubband pairing strength with visible regions of stability of ISP (intersubband paired state), ESP (equal subband paired state), and NS (normal state). Results are for $\mathbf{Q} = 0$ and a selected value of the energy separation $\Delta E = 5$ meV. (b) The region of stability of the Fulde-Ferrell intersubband state with values of the $\mathbf{Q}$ vector which minimize the free energy in the inset. Results are for $\mathbf{Q} \neq 0$ within the parameter range marked by the white rectangle in (a).

based on Eq. (8), whose explicit form is given by

$$\begin{aligned} \Gamma_{11(22)} &= V\Delta_{11(22)} + V_{12}\Delta_{22(11)}, \\ \Gamma_{12(21)} &= V_{12}\Delta_{12(21)} + V_{12}\Delta_{21(12)}. \end{aligned} \tag{12}$$

The terms with $V_{12}\Delta_{12(21)}$ and $V_{12}\Delta_{21(12)}$ correspond to the intersubband pairing, while $V_{12}\Delta_{22(11)}$ refers to the intersubband pair hopping. The latter is operative only when the intrasubband pairs are created ($\Delta_{11} \neq 0$ and $\Delta_{22} \neq 0$). In such a case and when the symmetry of the Cooper pair tunneling rate between the bands is lifted due to $\Delta E \neq 0$, the $V_{12}\Delta_{22(11)}$ term enhances the disproportion between the electron concentrations in the two subbands. This, in turn, strongly suppresses the intersubband pairing both in the form with zero total momentum of the Cooper pairs (ISP) and in the FF state [see Fig. 3(b)]. When the intersubband pair hopping is neglected, such strong competition does not occur, and the coexistence region of ESP and ISP appears, as shown in Ref. [49].

A detrimental impact of the intrasubband pairing on the IFF phase is clearly demonstrated in Fig. 3(b), which presents the results of calculations with the nonzero total momentum pairing included. The range of parameters (V_{12}, V) presented in Fig. 3(b) is marked by the white rectangle in Fig. 3(a). As we can see, in the narrow range of V the IFF stability region gradually decreases with increasing V due to their mutual competition described above. Note that the steplike character of the IFF stability region in Fig. 3(b) is a result of the relatively small resolution used in our calculations. It is due to the high computational costs required for the calculations with nonzero momentum pairing.

The influence of magnetic field for $V = 0.05$ is presented in Fig. 4. It should be noted that in the results presented so far all the paired states correspond to a spin-singlet, subband-triplet pairing with $\Delta_{ST} \neq 0$ and $\Delta_{TS} = 0$, where

$$\begin{aligned} \Delta_{ST} &= \frac{1}{\sqrt{2}}(\langle \hat{c}^{\dagger}_{1\uparrow}\hat{c}^{\dagger}_{2\downarrow}\rangle - \langle \hat{c}^{\dagger}_{2\uparrow}\hat{c}^{\dagger}_{1\downarrow}\rangle), \\ \Delta_{TS} &= \frac{1}{\sqrt{2}}(\langle \hat{c}^{\dagger}_{1\uparrow}\hat{c}^{\dagger}_{2\downarrow}\rangle + \langle \hat{c}^{\dagger}_{2\uparrow}\hat{c}^{\dagger}_{1\downarrow}\rangle). \end{aligned} \tag{13}$$

However, in the presence of external magnetic field, the Zeeman spin splitting may lead to $|\langle \hat{c}^{\dagger}_{1\uparrow}\hat{c}^{\dagger}_{2\downarrow}\rangle| \neq |\langle \hat{c}^{\dagger}_{2\uparrow}\hat{c}^{\dagger}_{1\downarrow}\rangle|$. This is caused by the fact that the two spin subbands corresponding to $|2,\uparrow\rangle$ and $|1,\downarrow\rangle$ are closer to each other than the two corresponding to $|1,\uparrow\rangle$ and $|2,\downarrow\rangle$. This mechanism is schematically presented in Fig. 4(e). As a result the spin-singlet, subband-triplet paired state is mixed with spin-triplet, subband-singlet state for which $\Delta_{ST} \neq 0$ and $\Delta_{TS} \neq 0$ [ISP* in the phase diagram in Fig. 4(a)]. The region of stability of such an exotic state appears for relatively large magnetic fields, as seen in Figs. 4(b) and 4(c); however, the Δ_{TS} component of the pairing amplitude is significantly smaller than Δ_{TS} [Fig. 4(d)]. Note that the ISP* phase leads to a reentrance of superconductivity with increasing field B in the range $0.06 \lesssim V_{12} \lesssim 0.1$, where the intersubband paired phase is formed after the intrasubband phase, already suppressed by the Zeeman splitting.

Our calculations with $\mathbf{Q} \neq 0$ in the presence of external magnetic field show that the Fulde-Ferrell phase can appear in both the inter- and intrasubband forms. The latter is created due to the compensation of the Fermi wave vector mismatch caused by the Zeeman splitting within the two bands [FF phase in Fig. 4(a)]. As presented in Fig. 1, in general the $\mathbf{Q}$ vectors for each of the subbands and between them could be different when $H \neq 0$. However, due to the fact that $\Delta E \ll \mu$ the wave vector mismatch induced by the magnetic field at the Fermi level is nearly the same for both the subbands, and therefore we assume $\mathbf{Q_1} = \mathbf{Q_2}$. The corresponding regions of stability of both phases are shown in Fig. 5, where the amplitude for the nonzero pairing between the subbands and within the subbands is plotted as a function of both V_{12} and B. Additionally, in Figs. 5(c) and 5(d) the values of the Cooper pair momentum which minimize the system energy are provided. Note that the ordinary FF phase induced by the Zeeman effect appears only at the border between the ESP phase and NS state. In contrast to that, the IFF phase emerges at both the NS/ISP* and ISP*/ISP borders.

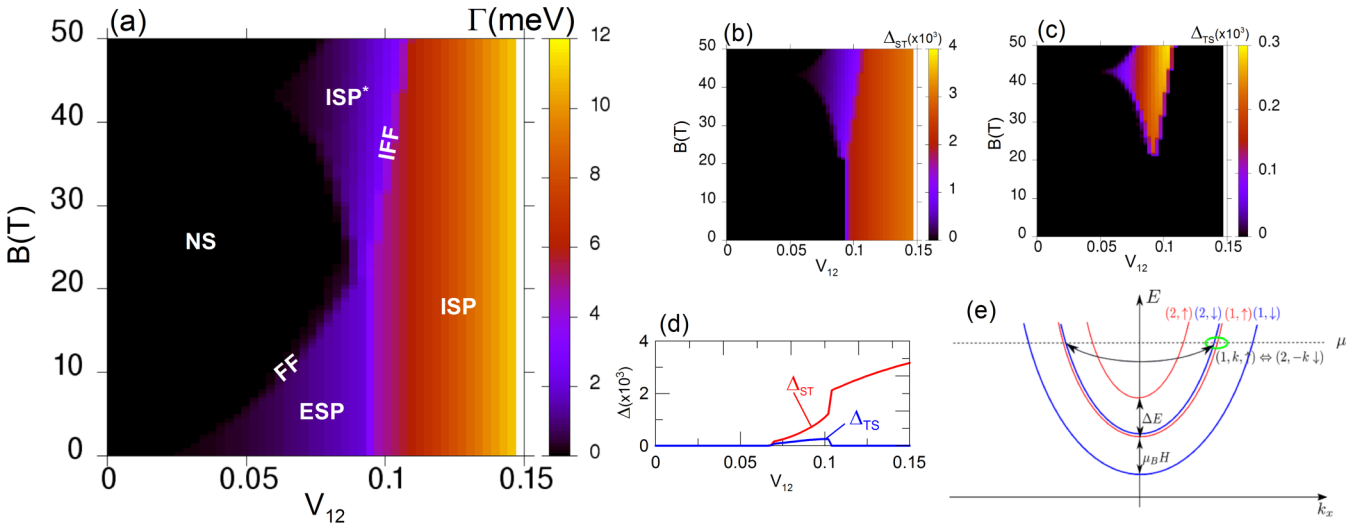

FIG. 4. (a) The phase diagram in the (V_{12}, B) plane for the selected value of the intrasubband pairing $V = 0.05$. (b) The spin-singlet, subband-triplet pairing amplitude and (c) the spin-triplet, subband-singlet pairing amplitude vs V_{12} and B. In (d) we show Δ_{ST} and Δ_{TS} as a function of V_{12} for a selected value of B. Additionally, in (e) the schematic representation of the spin-split subbands in the external magnetic field is provided.

IV. DISCUSSION

When it comes to the physical realization of the proposed intersubband superconducting phases, the important question concerns the balance between the inter- and intrasubband pairing strengths in real systems. Our paper shows that the intersubband FF phase appears only if the intersubband coupling is dominant. Note that both the inter- and intrasubband couplings in metallic nanofilms are determined by two factors: (i) the electron-phonon coupling and (ii) the matrix elements (physically, the overlap between the subbands). Determination of the electron-phonon coupling in individual subbands and between them in metallic nanofilms is still an open issue from both theoretical and experimental points of view. Recent experiments show that the electron-phonon constant varies from one band to another and might be different even for two neighboring subbands [53]. It is worth noting also that the relation between the electron-phonon constant and superconducting properties is not straightforward in nanostructures (e.g., electron-phonon coupling can be strongly enhanced due to surface and/or interface effects, defects, etc.). The same is true for the intersubband electron-phonon coupling, which is still unexplored for metallic nanofilms. Furthermore, the intersubband coupling can be strongly enhanced by the interaction matrix elements, which can be changed by all kinds of potential deformations. However, even if both factors (i) and (ii) appear in the system, the intersubband pairing is favorable when the subbands are energetically close to each other. This strongly suggests that the simplest way to make the intersubband pairing dominant is to apply the magnetic field. Then, the intrasubband pairing is gradually destroyed by the Zeeman splitting, but the same Zeeman effect shifts two different bands with opposite spins closer to each other, making the intersubband preferable. This mechanism is described in the last part of the previous section and schematically presented in Fig. 1(b). For this reason we believe that even in the situation with relatively small V_{12} and/or large ΔE the application of the magnetic field could allow for the experimental observation of the intersubband FF phase.

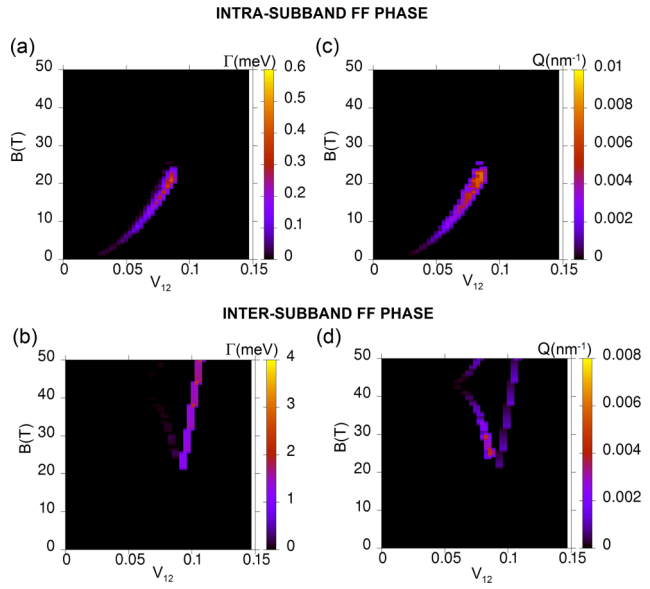

FIG. 5. The superconducting gaps corresponding to the nonzero momentum pairing (a) within the subbands and (b) between the subbands as functions of V_{12} and B. (c) and (d) The values of the Cooper pair momentum which minimize the system energy.

It should be noted that in superconducting low-dimensional structures the effect of fluctuations may play a role. Thermally activated phase slip and quantum phase slip are known to be significant in superconducting nanostructures, leading to difficulties in the description based on the mean-field theory. They result in a long tail appearing in the temperature dependence of the resistance below the critical temperature. However, as shown by recent experiments, such a tail is not observed for Pb

nanofilms with thickness down to 25 monolayers [3,13,14,16] for which the $\Delta(T)$ dependence exhibits the BCS-like behavior [13]. It has been suggested that such a situation is related to the substrate on which the nanofilms are grown, which may stabilize the superconducting state, making the quantum phase slip not pronounced. Furthermore, the BCS theory was, in fact, successfully applied to explain many experiments, and good quantitative agreement with the experimental data was found [18,54–56]. All this allows us to expect that the mean-field approach used in the paper is reasonable for the considered nanofilm geometry.

Although in our study we consider a particular case of a Pb metallic nanofilm, the appearance of a spontaneous Fulde-Ferrell state could be energetically favorable for any multiband superconductor such as MgB_2 [4–7] and iron-based superconductors [8–11,52]. In the latter, the bottoms of the bands (between which the pairing may appear) coincide; nevertheless, the Fermi wave vector mismatch appears due to a specific electronic structure. In general, the Fermi wave vector mismatch has to be relatively small for the IFF phase to appear in systems with a weak intersubband coupling constant. This can be seen in our calculations where the nonzero-momentum pairing emerged even for low V_{12} if ΔE was small. We propose that those conditions could also be satisfied in the two-dimensional superconducting electron gas created at $LaAlO_3/SrTiO_3$ interfaces [57–60] where the appearance of the intersubband pairing is confirmed experimentally [61] and can be controlled by gating (doping) [60]. However, the question of the pairing mechanism in this system still remains open, as well as the role of interelectronic correlations in stabilizing the superconducting state.

Another example of the realization of the proposed state is a system consisting of two types of particles with two different masses between which a pairing mechanism is realized. Such a scenario can take place in a two-component ultracold Fermi gas trapped in an optical lattice. Note that, since the existence of the IFF phase does not require any magnetic field, its appearance is independent of the Maki criterion for the Cooper pair decomposition, which plays an important role in the case of the conventional FF state. This significantly extends the range of materials in which this phase can possibly be observed.

V. SUMMARY

In the present paper, we have analyzed the intersubband pairing in freestanding Pb nanofilms where the subbands are created due to the quantization effect induced by the confinement in the growth direction. In order to determine the principal properties of the paired state we have used a model consisting of two parabolic subbands separated by the energy ΔE. Nonzero values of the energy are detrimental for the intersubband pairing as they generate a Fermi wave vector mismatch between the particles with opposite spins and momenta. However, as we showed here, such a mismatch between the bands can be compensated by the nonzero total momentum of the Cooper pairs, which leads to the appearance of the spontaneous Fulde-Ferrell intersubband state. The interesting feature of such a state is that it can be formed without the necessity of applying any external magnetic or electric field. Since the intersubband pair hopping processes together with the intrasubband pairing enhance the disproportion between the electron concentrations in the two bands, the coexistence of the inter- and intrasubband paired states does not appear. The same mechanism leads to suppression of the FF stability region with increasing intrasubband pairing.

Our calculations have shown that in relatively high external magnetic field, due to the Zeeman splitting of the bands, an exotic interband paired state appears, for which the spin-singlet, subband-triplet and spin-triplet, subband-singlet Cooper pairs are created. The appearance of such a phase has a reentrant character with increasing magnetic field after the intrasubband paired state is destroyed. The spontaneous intersubband Fulde-Ferrell phase appears in all of the analyzed situations close to the transition between the ISP phase and other states appearing in the phase diagram such as the normal state and the intrasubband paired state. Finally, we discussed the possibility of the existence of the IFF pairing in novel superconducting materials.

ACKNOWLEDGMENT

This work was supported by the National Science Centre, Poland (NCN), according to Decision No. 2017/26/D/ST3/00109 and in part by PL-Grid Infrastructure.

[1] T. Zhang, P. Cheng, W. J. Li, Y. J. Sun, X. G. Wang, G. Zhu, K. He, L. L. Wang, X. C. Ma, X. Chen, Y. Y. Wang, Y. Liu, H. Q. Lin, J. F. Jia, and Q. K. Xue, Nat. Phys. **6**, 104 (2010).

[2] T. Uchihashi, P. Mishra, M. Aono, and T. Nakayama, Phys. Rev. Lett. **107**, 207001 (2011).

[3] S. Qin, J. Kim, Q. Niu, and C. K. Shih, Science **324**, 1314 (2009).

[4] S. Souma, Y. Machida, T. Takahashi, H. Matsui, S. C. Wang, H. Ding, A. Kaminski, J. C. Campuzano, S. Sasaki, and K. Kadowaki, Nature (London) **423**, 65 (2003).

[5] F. Giubileo, D. Roditchev, W. Sacks, R. Lamy, D. X. Thanh, J. Klein, S. Miraglia, D. Fruchart, J. Marcus, and P. Monod, Phys. Rev. Lett. **87**, 177008 (2001).

[6] X. K. Chen, M. J. Konstantinović, J. C. Irwin, D. D. Lawrie, and J. P. Franck, Phys. Rev. Lett. **87**, 157002 (2001).

[7] P. Szabó, P. Samuely, J. Kačmarčík, T. Klein, J. Marcus, D. Fruchart, S. Miraglia, C. Marcenat, and A. G. M. Jansen, Phys. Rev. Lett. **87**, 137005 (2001).

[8] K. Kuroki, S. Onari, R. Arita, H. Usui, Y. Tanaka, H. Kontani, and H. Aoki, Phys. Rev. Lett. **101**, 087004 (2008).

[9] X. Dai, Z. Fang, Y. Zhou, and F.-C. Zhang, Phys. Rev. Lett. **101**, 057008 (2008).

[10] P. Jeglič, A. Potočnik, M. Klanjšek, M. Bobnar, M. Jagodič, K. Koch, H. Rosner, S. Margadonna, B. Lv, A. M. Guloy, and D. Arčon, Phys. Rev. B **81**, 140511(R) (2010).

[11] D. J. Singh and M.-H. Du, Phys. Rev. Lett. **100**, 237003 (2008).

[12] M. M. Özer, J. R. Thompson, and H. H. Weitering, Nat. Phys. **2**, 173 (2006).
[13] D. Eom, S. Qin, M. Y. Chou, and C. K. Shih, Phys. Rev. Lett. **96**, 027005 (2006).
[14] Y. Guo, Y. F. Zhang, X. Y. Bao, T. Z. Han, Z. Tang, L. X. Zhang, W. G. Zhu, E. G. Wang, Q. Niu, Z. Q. Qiu, J. F. Jia, Z. X. Zhao, and Q. K. Xue, Science **306**, 1915 (2004).
[15] X.-Y. Bao, Y.-F. Zhang, Y. Wang, J.-F. Jia, Q.-K. Xue, X. C. Xie, and Z.-X. Zhao, Phys. Rev. Lett. **95**, 247005 (2005).
[16] T. Sekihara, R. Masutomi, and T. Okamoto, Phys. Rev. Lett. **111**, 057005 (2013).
[17] A. A. Shanenko, M. D. Croitoru, and F. M. Peeters, Phys. Rev. B **78**, 024505 (2008).
[18] A. A. Shanenko, M. D. Croitoru, and F. M. Peeters, Phys. Rev. B **75**, 014519 (2007).
[19] P. Wójcik and M. Zegrodnik, J. Phys. Condens. Matter **26**, 455302 (2014).
[20] J. C. Nabity and M. N. Wybourne, Phys. Rev. B **44**, 8990 (1991).
[21] A. A. Shanenko, J. A. Aguiar, A. Vagov, M. D. Croitoru, and M. V. Milošević, Supercond. Sci. Technol. **28**, 054001 (2015).
[22] P. Fulde and A. Ferrell, Phys. Rev. **135**, A550 (1964).
[23] A. I. Larkin and Y. N. Ovchinnikov, Zh. Eksp. Teor. Fiz. **47**, 1136 (1964).
[24] M. M. Maśka, M. Mierzejewski, J. Kaczmarczyk, and J. Spałek, Phys. Rev. B **82**, 054509 (2010).
[25] A. Ptok and D. Crivelli, J. Low Temp. Phys. **172**, 226 (2013).
[26] A. Ptok, Eur. Phys. J. B **87**, 2 (2014).
[27] M. Takahashi, T. Mizushima, and K. Machida, Phys. Rev. B **89**, 064505 (2014).
[28] L. W. Gruenberg and L. Gunther, Phys. Rev. Lett. **16**, 996 (1966).
[29] J. Singleton, J. A. Symington, M. S. Nam, A. Ardavan, M. Kurmoo, and P. Day, J. Phys. Condens. Matter **12**, L641 (2000).
[30] M. A. Tanatar, T. Ishiguro, H. Tanaka, and H. Kobayashi, Phys. Rev. B **66**, 134503 (2002).
[31] S. Uji, T. Terashima, M. Nishimura, Y. Takahide, T. Konoike, K. Enomoto, H. Cui, H. Kobayashi, A. Kobayashi, H. Tanaka, M. Tokumoto, E. S. Choi, T. Tokumoto, D. Graf, and J. S. Brooks, Phys. Rev. Lett. **97**, 157001 (2006).
[32] J. Shinagawa, Y. Kurosaki, F. Zhang, C. Parker, S. E. Brown, D. Jerome, K. Bechgaard, and J. B. Christensen, Phys. Rev. Lett. **98**, 147002 (2007).
[33] P. Wójcik and M. Zegrodnik, Phys. E (Amsterdam, Neth.) **83**, 442 (2016).
[34] M. D. Croitoru, M. Houzet, and A. I. Buzdin, Phys. Rev. Lett. **108**, 207005 (2012).
[35] M. D. Croitoru and A. I. Buzdin, Phys. Rev. B **86**, 064507 (2012).
[36] A. Bianchi, R. Movshovich, C. Capan, P. G. Pagliuso, and J. L. Sarrao, Phys. Rev. Lett. **91**, 187004 (2003).
[37] K. Kumagai, M. Saitoh, T. Oyaizu, Y. Furukawa, S. Takashima, M. Nohara, H. Takagi, and Y. Matsuda, Phys. Rev. Lett. **97**, 227002 (2006).
[38] V. F. Correa, T. P. Murphy, C. Martin, K. M. Purcell, E. C. Palm, G. M. Schmiedeshoff, J. C. Cooley, and S. W. Tozer, Phys. Rev. Lett. **98**, 087001 (2007).
[39] Y. Matsuda and H. Shimahara, J. Phys. Soc. Jpn. **76**, 051005 (2007).
[40] P. Wójcik, M. Zegrodnik, and J. Spałek, Phys. Rev. B **91**, 224511 (2015).
[41] M. Mika and P. Wójcik, J. Phys.: Condens. Matter **29**, 475302 (2017).
[42] J. Wang, Y. Che, L. Zhang, and Q. Chen, Phys. Rev. B **97**, 134513 (2018).
[43] G. Koutroulakis, H. Kühne, J. A. Schlueter, J. Wosnitza, and S. E. Brown, Phys. Rev. Lett. **116**, 067003 (2016).
[44] R. Beyer, B. Bergk, S. Yasin, J. A. Schlueter, and J. Wosnitza, Phys. Rev. Lett. **109**, 027003 (2012).
[45] H. Mayaffre, S. Krämer, M. Horvatić, C. Berthier, K. Miyagawa, K. Kanoda, and V. F. Mitrović, Nat. Phys. **10**, 928 (2014).
[46] A. I. Buzdin, Rev. Mod. Phys. **77**, 935 (2005).
[47] A. Hart, H. Ren, M. Kosowsky, G. Ben-Shach, P. Leubner, C. Brüne, H. Buhmann, L. W. Molenkamp, B. I. Halperin, and A. Yacoby, Nat. Phys. **13**, 87 (2017).
[48] A. Q. Chen, M. J. Park, S. T. Gill, Y. Xiao, D. R. Plessis, G. J. MacDougall, M. J. Gilbert, and N. Mason, Nat. Commun. **9**, 3478 (2018).
[49] A. Moreo, M. Daghofer, A. Nicholson, and E. Dagotto, Phys. Rev. B **80**, 104507 (2009).
[50] C. M. Wei and M. Y. Chou, Phys. Rev. B **66**, 233408 (2002).
[51] M. Zegrodnik and J. Spałek, J. Supercond. Novel Magn. **28**, 1155 (2015).
[52] M. Zegrodnik and J. Spałek, Phys. Rev. B **90**, 174507 (2014).
[53] A. V. Matetskiy, S. Ichinokura, L. V. Bondarenko, A. Y. Tupchaya, D. V. Gruznev, A. V. Zotov, A. A. Saranin, R. Hobara, A. Takayama, and S. Hasegawa, Phys. Rev. Lett. **115**, 147003 (2015).
[54] Y. Chen, A. A. Shanenko, and F. M. Peeters, Phys. Rev. B **85**, 224517 (2012).
[55] D. Valentinis, D. van der Marel, and C. Berthod, Phys. Rev. B **94**, 054516 (2016).
[56] P. Wójcik and M. Zegrodnik, Phys. Status Solidi B **251**, 1069 (2014).
[57] A. Joshua, S. Pecker, J. Ruhman, E. Altman, and S. Ilani, Nat. Commun. **3**, 1129 (2012).
[58] N. Reyren, S. Thiel, A. D. Caviglia, L. Fitting Kourkoutis, G. Hammerl, C. Richter, C. W. Schneider, T. Kopp, A. S. Rüetschi, D. Jaccard, M. Gabay, D. A. Muller, J. M. Triscone, and J. Mannhart, Science **317**, 1196 (2007).
[59] M. S. Scheurer and J. Schmalian, Nat. Commun. **6**, 6005 (2015).
[60] T. V. Trevisan, M. Schütt, and R. M. Fernandes, Phys. Rev. Lett. **121**, 127002 (2018).
[61] G. Singh, A. Jouan, G. Herranz, M. Scigaj, F. Sanchez, L. Benfatto, S. Caprara, M. Grilli, G. Saiz, F. Couedo, C. Feuillet-Palma, J. Lesueur, and N. Bergeal, arXiv:1806.02212.